High-Voltage Charging-Induced Strain, Heterogeneity, and Micro-Cracks in Secondary Particles of a Nickel-Rich Layered Cathode Material

Yuwei Mao, Xuelong Wang, Sihao Xia, Kai Zhang, Chenxi Wei, Seongmin Bak, Zulipiya Shadike, Xuejun Liu, Yang Yang, Rong Xu, Piero Pianetta, Stefano Ermon, Eli Stavitski, Kejie Zhao, Zhengrui Xu, Feng Lin, Xiao-Qing Yang,* Enyuan Hu,* and Yijin Liu*

Nickel-rich layered materials $LiNi_{1-x-y}Mn_xCo_yO_2$ are promising candidates for high-energy-density lithium-ion battery cathodes. Unfortunately, they suffer from capacity fading upon cycling, especially with high-voltage charging. It is critical to have a mechanistic understanding of such fade. Herein, synchrotron-based techniques (including scattering, spectroscopy, and microcopy) and finite element analysis are utilized to understand the $LiNi_{0.6}Mn_{0.2}Co_{0.2}O_2$ material from structural, chemical, morphological, and mechanical points of view. The lattice structural changes are shown to be relatively reversible during cycling, even when 4.9 V charging is applied. However, local disorder and strain are induced by high-voltage charging. Nano-resolution 3D transmission X-ray microscopy data analyzed by machine learning methodology reveal that high-voltage charging induced significant oxidation state inhomogeneities in the cycled particles. Regions at the surface have a rock salt–type structure with lower oxidation state and build up the impedance, while regions with higher oxidization state are scattered in the bulk and are likely deactivated during cycling. In addition, the development of micro-cracks is highly dependent on the pristine state morphology and cycling conditions. Hollow particles seem to be more robust against stress-induced cracks than the solid ones, suggesting that morphology engineering can be effective in mitigating the crack problem in these materials.

1. Introduction

The massive consumption of fossil energy and the associated environmental deterioration have led to global concerns and called for renewable energy. Energy storage is a vital component in the landscape of energy because it is the key part for all types of renewable energy, including solar, wind, and geothermal energies. Lithium ion batteries are becoming more and more important energy storage technology in consumer electronics and electric vehicles (EVs).[1–3]

Affordable EVs put stringent requirements on their power batteries, including high energy density, high power density, long cycle/calendar life, and low cost. The performance of batteries is closely related to the properties of the cathode materials used. Layered $LiNi_{1-x-y}Mn_xCo_yO_2$ (NMC) material emerges as a practical cathode material due to its balanced good properties, including high reversible capacity ($\approx$200 mAh g^{-1})[4,5] and low cost compared to commonly used

Y. Mao, S. Xia, Dr. K. Zhang, C. Wei, Prof. P. Pianetta, Dr. Y. Liu
Stanford Synchrotron Radiation Light Source
SLAC National Accelerator Laboratory
Menlo Park, CA 94025, USA
E-mail: liuyijin@slac.stanford.edu

Y. Mao, Prof. X. Liu
School of Computer Science and Technology
Nanjing University of Aeronautics and Astronautics
Nanjing 211100, Jiangsu, China

X. Wang, Dr. S. Bak, Dr. Z. Shadike, Dr. X.-Q. Yang, Dr. E. Hu
Chemistry Division
Brookhaven National Laboratory
Upton, NY 11973, USA
E-mail: xyang@bnl.gov; enhu@bnl.gov

Dr. K. Zhang
Beijing Synchrotron Radiation Facility
Institute of High Energy Physics
Chinese Academy of Sciences
Beijing 100049, China

Dr. Y. Yang
European Synchrotron Radiation Facility
38000 Grenoble, France

R. Xu, Prof. K. Zhao
School of Mechanical Engineering
Purdue University
West Lafayette, IN 47906, USA

Prof. S. Ermon
Department of Computer Science
Stanford University
Stanford, CA 94305-2205, USA

1900247 (1 of 11)

**ADVANCED
SCIENCE NEWS**
www.advancedsciencenews.com

**ADVANCED
FUNCTIONAL
MATERIALS**
www.afm-journal.de

cathode material $LiCoO_2$.[6–8] Among NMC families, materials with high Ni content (Ni-rich NMC) have become the focus of the current research because of the improvement in the specific capacity.[6,9,10] However, Ni-rich NMC material is reported to suffer from relatively poor high-voltage stability compared to compounds with lower Ni content.[11,12] Besides, significant capacity fading during cycling has been observed in Ni-rich NMC.[13] The EV application calls for battery solutions with emphasis on power and energy density to deliver high accelerating power and long driving range, which demand the capability of high-voltage operation. Therefore, it is very important to investigate the degradation mechanism of Ni-rich NMC materials during high-voltage cycling.

The transition metal elements Ni, Mn, and Co contribute to the performance of NMC in different ways. Ni is responsible for most of the charge compensation, Mn is highly related to the structural integrity and thermal stability,[10,14] while Co helps stabilizing layered structure.[15,16] The dissolution of transition metal into electrolyte has been revealed as an important factor contributing to material degradation during high-voltage cycling for Ni-rich NMC materials.[3,17–19] Dissolved transition metal ions accelerate capacity fading through formation of passivation layer on both cathode and anode material.[20,21] Besides metal dissolution, other factors may also aggravate degradation. In our previous publications, it was shown that for $LiCoO_2$ particles, charge-state heterogeneity can be generated through electrochemical cycling.[22,23] For multi-element materials like NMC, the heterogeneity could be even more serious. Charge-state heterogeneity has been observed in NMC333 particle and was reported to be persistent even after the particle was fully relaxed.[24] Unfortunately, the heterogeneity in NMC particles upon high-voltage cycling, especially for Ni-rich NMC, has not been systematically studied. Furthermore, although the role of surface reconstruction in Ni-rich NMC degradation has been studied and reported in the literature,[11,25,26] the effects of charge-state heterogeneity on performance degradation of Ni-rich NMC materials have not been thoroughly investigated and reported. Here, we report our experimental observation and try to establish connections between inhomogeneity (chemical and morphological) and performance fading of NMC622 material, especially at high-voltage charging condition.

In heterogeneous materials, local oxidation states of transition metals can be significantly deviated from the bulk average and the local electrochemical reactions can be quite different from the bulk average. These chemical "outliers" bring big challenges for characterization of heterogeneity, since they are usually small in the total population and sparse in the spatial distribution. The conventional bulk-averaged techniques are, therefore, not sensitive to these "outliers," as the bulk signal is dominated by the majority of the material. However, the effects of these "outliers" on performance degradation might be very important, sometime even critical. Experimental probes with sufficient spatial resolution and good chemical sensitivity are needed to reveal the effects of local "outliers" on the macroscopic performance.[27] Such an approach also requires advanced computing methods to efficiently analyze large amount of experimental datasets and reduce its dimensionality in a supervised, unsupervised, or hybrid manner.[28] These techniques were utilized in this study.

In this work, Ni-rich NMC material with composition of $LiNi_{0.6}Mn_{0.2}Co_{0.2}O_2$ (NMC622) was chosen as a representative.[29] Samples with multiple cycle histories over different voltage windows (3–4.4, 3–4.6, and 3–4.9 V) were studied. On the one hand, high-voltage charging does not induce obvious lattice structural change. It does not result in oxygen release from the lattice either. On the other hand, it does lead to the formation of strain, charge-state inhomogeneity, and morphological defects. Such inhomogeneity and the consequently induced micro-cracks are believed to be responsible for the capacity fading during high-voltage charging. Through a machine-learning approach developed herein, we are able to identify and visualize the outliers in the particles with high-voltage cycling history (over the voltage windows of 3–4.6 and 3–4.9 V). Visualization of the spatial distribution of these outliers suggests that more-reduced and more-oxidized regions coexist, showing the inhomogeneity of the high-voltage cycled particles in oxidation state. The formation and evolution of these local outliers might be the origins for cycling-induced mechanical strain (as is evident from the bulk X-ray diffraction [XRD] data), which eventually triggered the formation of micro-cracks in the cycled particles. Based on these results, a possible mitigation strategy is proposed and discussed.

2. Results and Discussion

Scanning electron microscopy images (Figure S1, Supporting Information) show that the pristine NMC622 secondary particles are in spherical shape with diameter around 10 μm. Each secondary particle is composed of nano-sized primary particles (approximately hundreds of nanometers). Synchrotron XRD data indicate that the pristine material has a pure layered structure with the symmetry described by the $R\bar{3}m$ space group (Figure S2, Supporting Information). By using Rietveld refinement, detailed structural information is extracted and shown in Table S1, Supporting Information. Li atoms mostly occupy the 3a site (0, 0, 0), transition metals (Ni, Mn, and Co) mostly occupy the 3b site (0, 0, 0.5), while oxygen atoms occupy the 6c site (0, 0, 0.241). There is around 2.6% cation mixing between Li and transition metal (presumably Ni) according to the Rietveld refinement result. To gain insight into the valence state of each transition metal element, X-ray absorption near edge structure (XANES) were used and the results show that Ni is somewhere between divalent and trivalent, Co is trivalent, and Mn is tetravalent (Figure S3, Supporting Information) for the pristine sample.

The cathode using NMC622 material was assembled into cells to test the electrochemical performance in various cycling

Dr. E. Stavitski
National Synchrotron Light Source II
Brookhaven National Laboratory
Upton, NY 11973, USA
Z. Xu, Prof. F. Lin
Department of Chemistry
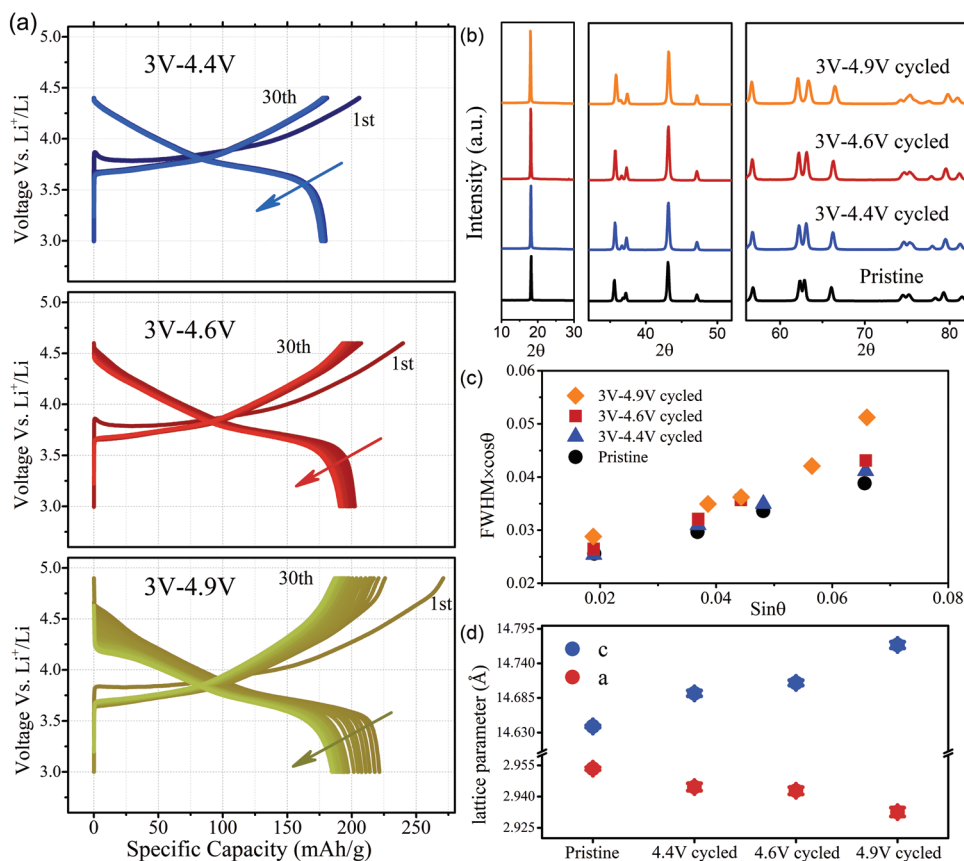Virginia Tech
Blacksburg, VA 24061, USA

**ADVANCED
SCIENCE NEWS**
www.advancedsciencenews.com

**ADVANCED
FUNCTIONAL
MATERIALS**
www.afm-journal.de

Figure 1. a) Electrochemical cycling at various voltage windows, b) ex situ XRD of NMC622 at discharged state after cycling in different voltage windows, c) the Williamson–Hall plot of the various cycled samples, and d) lattice parameters of NMC622 cycled with different charging cut-off voltage from Rietveld refinement.

voltage windows. Charging the material to high voltage is a common strategy to utilize the high-energy-density potential of high-nickel-content materials. The cells were cycled at a rate of C/8 (about 0.11 mA cm^{-2} current density) to different charge cut-off voltages (4.4, 4.6, and 4.9 V, respectively) but the same discharge cut-off voltage (3 V). The charge–discharge curves are shown in **Figure 1**a. The NMC622 material shows a typical sloping charge profile which indicates a solid–solution-type reaction. The cycling performance is closely related to the charge cut-off voltage. When NMC622 is cycled between 4.4 and 3 V, it can deliver a capacity of around 175 mAh g^{-1} with excellent reversibility. When the charge voltage is increased to 4.6 V, the delivered capacity of the first cycle can be as large as 200 mAh g^{-1}. However, it starts to show significant capacity fade upon cycling. Increasing the charge voltage to 4.9 V can further increase the capacity, but it rapidly decreased from 225 mAh g^{-1} for the 1st cycle to only 180 mAh g^{-1} for the 30th cycle. Furthermore, the over potential between charging and discharging processes is proportional to the charge cut-off voltage, indicating faster impedance growth at higher charge cut-off voltage. The long-term cycling performance of NMC622 material is tested by cycling the cell between 2.8 and 4.5 V with 1C charging and discharging current (≈0.9 mA cm^{-2}) at room temperature. The results are shown in Figure S4, Supporting Information, and are comparable to those reported in recent literatures.[30–33]

Previously, such capacity fade was proposed to be caused mainly by the irreversible lattice structural changes.[34,35] However, our ex situ XRD results for NMC622 materials at different voltages show generally reversible changes during all charge–discharge processes at different charge voltage limits (Figure 1b). The well-preserved XRD features indicate that the average lattice structure of NMC622 material is almost intact against deep delithiation, or high-voltage charge. Even when NMC622 goes through a 5.2–3 V cycle, all the peaks in the pristine XRD pattern are well recovered in the discharged XRD data with no extra peaks observed. The pattern for sample at 5.2 V charged state (Figure S2b, Supporting Information) is much alike that of the highly delithiated LiNiO$_2$.[36] Therefore, the accelerated degradation of the material performance through high-voltage charge is unlikely due to the irreversible global lattice structural damages. However, a closer look at the XRD patterns reveals that the peaks are broadened for the cycled samples. This is clearly seen from the Williamson–Hall (W–H) plot which is shown in Figure 1c. In the W–H plot, the full width at half maximum (FWHM) of the Bragg peak is multiplied by cosθ and plotted as a function of sinθ. In this way, the strain of the sample is indicated by the slope of the extrapolated line, and the size of coherent domain is indicated by the interception of the line on the *y*-axis.[37] It clearly shows that cycling the NMC622 material through higher-voltage charge induces larger strain in

the structure. The build-up of the mechanical strain is believed to be responsible for the development of cracks and charge heterogeneity inside particles.[8,13,38] Other structural information was obtained through Rietveld refinement of XRD results. Figure 1d shows the dependence of lattice parameters of cycled NMC622 materials on the charging voltage limit. Lattice parameter *a* decreases as the charging cut-off voltage increases while lattice parameter *c* increases. Previous in situ XRD results showed that lattice parameters are closely related to the state-of-charge, or the Li content in NMC materials.[39–41] Generally, as the Li content decreases, lattice parameter *a* decreases and lattice parameter *c* increases. Smaller *a* parameter and larger *c* parameter can be associated with less Li content. Figure 1d indicates that NMC622 cannot be fully lithiated after multiple cycles. When a higher charging voltage is applied, less lithiation can be achieved during discharging. This is an evidence of the loss of active Li caused by cycling. Atomic displacement parameter (ADP), which is a measure of the structural disorder, was also fitted and the ADP at transition metal site is shown in Figure S5, Supporting Information. It indicates that when a higher charging voltage is applied, more structural disorder is induced in the cycled samples. Therefore, to understand the NMC material's degradation mechanism upon cycling to high charge cut-off voltage, we need to investigate the relationship between the mechanical strain and chemical inhomogeneity at the particle level.

In addition to the changes in the lattice structure as suggested by XRD patterns, the reaction of different transition metal elements during high-voltage cycling is investigated using X-ray absorption spectroscopy (XAS). Results of the XAS measurements on the pristine and cycled samples are shown in **Figure 2**. The XANES in Figure 2a shows that, after multiple cycling, the average oxidation state of Ni, Co, and Mn are mostly the same as those in the pristine samples. Surprisingly, this is even true for the 4.9–3 V cycled samples. These results suggest that there should be no obvious oxygen release from the bulk when this material is charged to high voltage. This is very different from the Li-rich NMC in which oxygen release from the bulk is a serious problem.[42] In contrast, the extended X-ray absorption fine structure (EXAFS) data, which are more sensitive to local chemical and structural changes, show amplitude reduction for the metal–oxygen and metal–metal peaks. To gain better understanding on this observation, the EXAFS patterns (Figure 2b) are fitted against the layered lattice structure model. The results show that the Debye–Waller factor, which is an indicator of the local structural disorder, keeps increasing with rising charge cut-off voltage for the Ni's data (Figure 2c), while those of the Co and Mn show much less variation. This indicates that local lattice structure around Ni atom is likely to change more severely than that of Co and Mn, suggesting that Ni is mainly responsible for the increased strain. Such mechanism clearly tells us that a more detailed microscopic
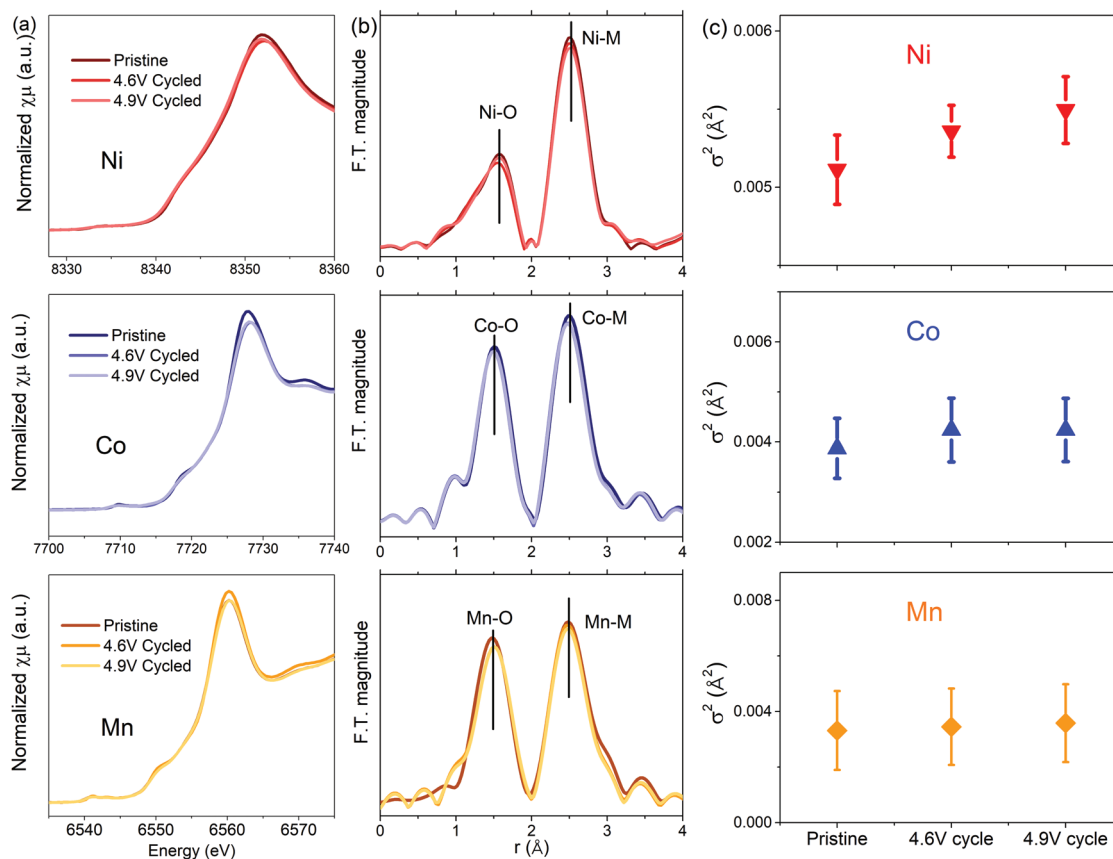

Figure 2. a) XANES and b) EXAFS of the pristine and the cycled samples. c) Fitted Debye–Waller factor change upon cycling for Ni, Co, and Mn.

investigation of the subparticle-level spatial variation of Ni's oxidation state is needed.

As suggested by the detailed analysis of XRD and XAS data, an in-depth particle-level microscopic study with chemical sensitivity is highly necessary. Although the primary particles are the fundamental units of the NMC622 material, the secondary particles are no less important from a practical perspective, since they are architectural building blocks of the electrode. In the secondary particles, defects such as grain boundaries and pores exist throughout the entire particle. Such defects are closely related to the build-up and evolution of mechanical strain and chemical heterogeneity.[43] Therefore, synchrotron-based nanoresolution spectro-microscopy study was carried out with a nominal spatial resolution at ≈30 nm to resolve the subparticle structural and chemical defects.[44] By coupling the energy scan with full-field imaging method, we can effectively collect nearly 1 million (1024 × 1024 pixels per field of view) spatially resolved XANES spectra at Ni K-edge over the course of ≈15 min.[45] On the one hand, such spectro-microscopic dataset contains valuable information for revealing the morphological and chemical characteristics of secondary particles. On the other hand, the volume and the complexity of the dataset cause challenges for

analysis and interpretation. In our previous works on LiCoO$_2$ material, machine-learning approaches were proven to be effective in extracting key information from huge datasets.[23] When prior knowledge of the anticipated chemical species in the system is available, a supervised machine-learning approach can be used to map out the spatial distribution of these chemical species.[28] When unknown chemical species could exist, more sophisticated clustering algorithms need to be implemented to conduct the search in an unsupervised manner.[45] Unanticipated chemical "outliers" can be identified and mapped out, helping us to discover new reaction paths and mechanisms.[23]

In this work, a hybrid supervised and unsupervised machine-learning approach is developed to identify and visualize the chemical outliers in the NMC622 particles at the discharged state. These NMC particles have gone through 30 cycles over different voltage windows. As discussed above (Figure 1a), the battery that was cycled between 3 and 4.4 V showed only negligible capacity fade, suggesting that the reactions occurred in this voltage window are of good reversibility. An unsupervised machine-learning algorithm was implemented to conduct a clustering analysis of the spectro-microscopic data over particles that were cycled between 3 and 4.4 V. **Figure 3** shows
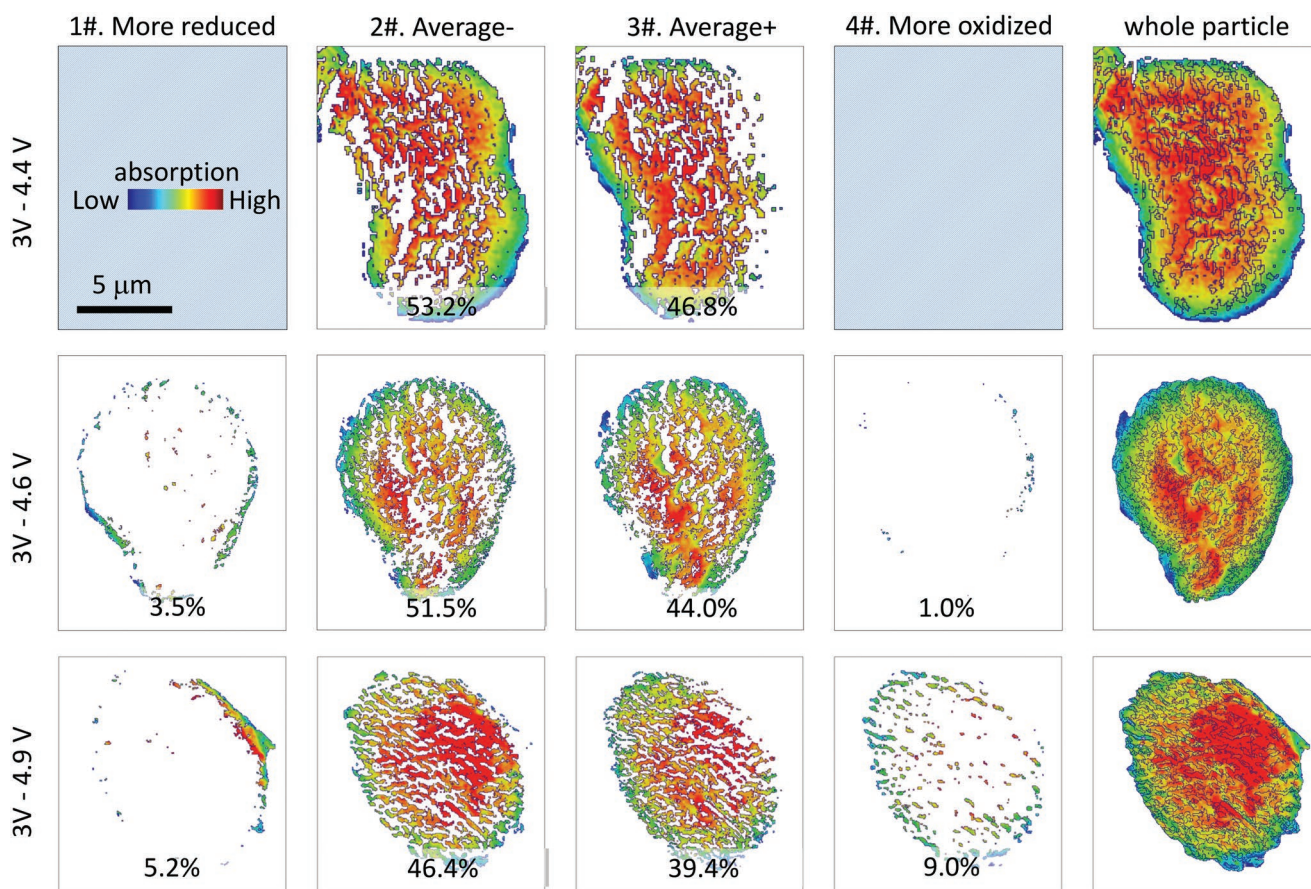

Figure 3. 2D mapping of mesoscale SOC heterogeneity in NMC secondary particles that were cycled over different voltage windows. In addition to the anticipated reduced and oxidized domains (2# and 3#), the machine-learning approach developed in this work identified two types of the chemical outliers in the particles cycled between 3 and 4.6 V and 3 and 4.9 V. While the more-reduced domains 1# mostly occur on the particle surface, the more-oxidized domains (4#) randomly distribute in the particle. The transmission images of the whole particles are shown in the right column. The area percentage of each cluster is shown in the corresponding inset. The scale bar in the upper left panel is 5 µm and is applicable to all panels. The color scheme represents the amount of X-ray attenuation at the corresponding pixels.

**ADVANCED
SCIENCE NEWS**
www.advancedsciencenews.com

**ADVANCED
FUNCTIONAL
MATERIALS**
www.afm-journal.de

the 2D projection images of representative NMC622 particles that are categorized into different clusters. As shown in the top row, two clusters (denoted 2# and 3#) were identified with distinctive spectroscopic fingerprints for particles cycled between 3 and 4.4 V (Figure S6, Supporting Information). These two clusters (2# and 3#) are correlated with two different oxidation states of Ni with 2# as more-reduced average oxidation state (average−) and 3# as more-oxidized average oxidation state (average+). The random distribution of the average+ (3#) and average− (2#) within the secondary particle shows the charge heterogeneity at the particle level. Since Ni is mainly responsible for the charge compensation during electrochemical cycling, the heterogeneous distribution of Ni oxidation states indicates non-uniform Li distribution within the particle, which is in good agreement with previous reports in similar systems.[24] The clustering result is then used as the training dataset to facilitate a supervised machine learning procedure to process the data from particles that were cycled more aggressively. Spectra with similar characteristics to one of the two clusters (2# and 3#, identified in the 3–4.4 V cycled particles) are assigned to the corresponding group, while the ones that are sufficiently different are labeled as chemical outliers. All the chemical outliers go through another round of unsupervised clustering, resulting in the separation of two groups, the more-reduced-than-average (1#) and the more-oxidized–than-average (4#) groups in Figure 3 (the corresponding spectroscopic fingerprints can be found in Figure S6, Supporting Information). More details regarding the hybrid supervised and unsupervised machine-learning approach can be found in Figures S7–S9, Supporting Information.

We observed both of the more-reduced and the more-oxidized domains in the particles that were cycled in voltage windows of 3–4.6 and 3–4.9 V. While the more-reduced domains (1#) seem mainly distributed at the surface of secondary particle, in contrast, the more-oxidized domains (4#) are not confined to the surface but scattered inside the particle as isolated domains. It is worthwhile to note that in the 3–4.6 V cycled particle, the amount of the more-oxidized domains is rather small (≈1%). To avoid any uncertainties in the domain locations deduced from the 2D XANES mapping results, 3D XANES mapping results are shown in **Figure 4** for an arbitrarily selected particle that was

cycled between 3 and 4.9 V. Through comparison between 3D rendering of chemical domains' spatial distribution (Figure 4a) and the corresponding virtual slices through the particle center (Figure 4b,c), the more-reduced domains 1# (blue, also highlighted by black arrows) are indeed located on the particle surface. In contrast, the more-oxidized domains 4# (yellow) are scattered all over the particle and are isolated from one another. The more-reduced domains 1# is close to Ni^{2+} (as suggested by its spectroscopic finger print) and mainly appearing on the secondary particle surface (up to ≈200 nm thick). A rather confined and concentrated distribution of cluster 1# in a thin layer on the surface is presented in the current observation (marked by color blue in Figure 4). Therefore, its origin could be attributed to the widely studied surface reconstruction in NMC materials. We point out here that, due to the limitation in the spatial resolution of the X-ray spectro-tomography technique, the conventionally defined "particle surface" with a thickness of a few atomic layers cannot be resolved in our data. The over-reduced local valence state of Ni within the blue layer in Figure 4, however, suggests that there is a depth-dependent pattern at the mesoscale, that is, the secondary particle scale where the region near the surface experiences more severe undesired lattice structure transformation from layered structure to NiO-like rock salt phase.[12,25,26] This layer could hinder diffusion pathways of the charge carriers and could impede the particle's contribution to the cell level electrochemistry. In particles cycled between 3 and 4.9 V, larger proportions of more-reduced domains 1# are observed than that in particles cycled between 3 and 4.6 V. It implies that high-voltage cycling would aggravate surface reconstruction. As for the more-oxidized domains 4#, although the average of the sample is at discharged state, these local domains seem to remain at more oxidized state and are not fully contributing to the capacity.[46] They are very likely no longer electrochemically active during subsequent cycling. Deactivation of material could be caused by irreversible local lattice structural changes, isolation from conducting network, or even segregation of transition metal cations. Actually, similar disconnected grains are observed inside other Ni-rich cathode material particles and are reported to be partly responsible for the capacity loss.[47,48] Comparing the portion of more-oxidized
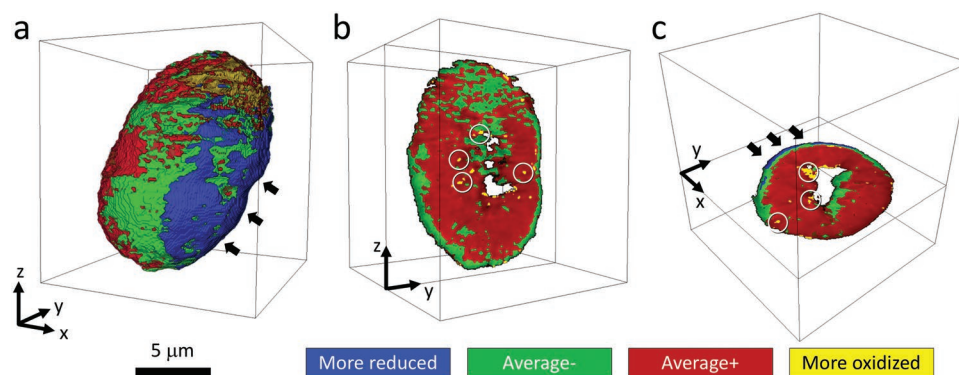

Figure 4. 3D distribution of the SOC within an NMC secondary particle that was cycled over a voltage window of 3–4.9 V. a) 3D rendering of different domains, color coded according to the legend on the bottom of the figure. The non-transparent visualization in (a) highlights the chemical complexity over the surface of the secondary particle. b,c) Virtual slices over the center of the particle in different orientations (in *yz* and *xy* planes, respectively). The white circles in (b) and (c) highlight the isolated more-oxidized domains 4# that scatter over the whole particle. The black arrows in (a) and (c) point to the more-reduced domains 1#, which appear on the particle surface.

domains 4# in particle cycled between 3 and 4.6 V and between 3 and 4.9 V, it can be clearly seen that more domains are deactivated with higher cycling voltages. It could be caused by large mechanical strain induced by high-voltage cycling and the large unit cell volume change of Ni-rich material when deeply delithiated.[13,36,49] It has been reported that severe lattice change induced by high-voltage charging may cause irreversible formation of intragranular dislocations and cracks.[50] In fact, the more-oxidized domains 4# we observed are quite small and are very likely initiated by the intragranular cracks. It should be noted that local deactivation may not be exclusively indicated by the regional more-oxidized domains 4# in a discharged particle. The deactivated parts could be in different oxidization states. Mapping out all these regions require more in-depth analysis and will be carried out in future studies. Some parts of the particle being deactivated indicates that non-uniform delithiation process occurs throughout the secondary particles. High-voltage cycling would intensify this heterogeneity and cause isolation of more domains, which eventually accelerate the capacity fading with cycling.

Moreover, it is worth pointing out that the blue domains (1#) do not cover the entire particle in Figure 4, possibly due to non-uniform electronic contact and electrolyte wetting over the particle surface. It has been reported that the electrolyte is a key player that critically affects the particle's surface chemistry.[26,51] The non-uniform development of the more-reduced domains 1# on particle surface causes the deterioration of the charge carriers' diffusion pathway, which, in turn, could further aggravate charge heterogeneity inside the particle leading to increased more-oxidized domains 4#, as highlighted by the white circles. This is in good agreement with the observation in 2D maps shown in Figure 3.

With the aid of machine-learning approach, XANES mapping provide insights on the subparticle-level chemical heterogeneity. Some unanticipated chemical species in the high-voltage cycled particles are closely related to the surface reconstruction and local deformation. These defects have been reported to cause morphology degradation, including the formation of cracks.[25] In **Figure 5**, the nano-resolution X-ray tomographic images of four particles that have gone through different cycling history are shown. The 3D rendering of the particles are shown in the left column with a few virtual slices in the middle. The right column of Figure 5 displays the void space within the
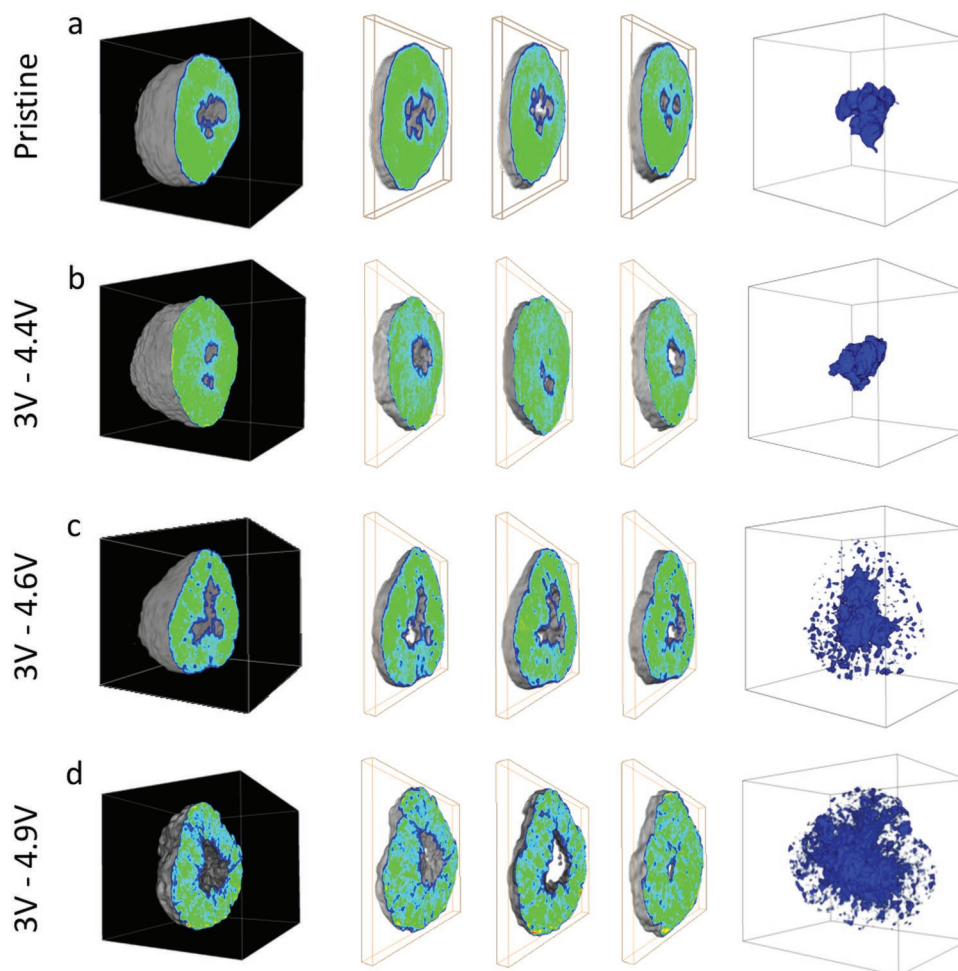

Figure 5. Evolution of the particle morphology upon cycling over different voltage windows. The left column is 3D renderings of the secondary particle structure. The middle columns are the virtual slices through different depths of the particle. The right column is the 3D rendering of the void volume (in blue) within the secondary particles. All the particles are about 8–10 microns in diameter.

ADVANCED
SCIENCE NEWS
www.advancedsciencenews.com

ADVANCED
FUNCTIONAL
MATERIALS
www.afm-journal.de

corresponding secondary particles. In both the pristine particle (Figure 5a) and the particle that was cycled between 3 and 4.4 V (Figure 5b), only the central hole is observed, suggesting that no morphological defects were detected upon cycling with relatively low charge cut-off voltage. More isolated void space is, however, seen in the particle cycled between 3 and 4.6 V (Figure 5c). Further increment in the charge cut-off voltage to 4.9 V leads to the formation of even more morphological defects, which visually appear to be interconnected crack network (Figure 5d). Large fractions of pores expose many new fresh material surfaces to the liquid electrolyte and could induce solid electrolyte interphase formation inside of the secondary particle, which could in turn intensify the heterogeneity and cause further morphological degradation. These morphological defects interplay with the chemical defects as discussed before, self-feed, and synergistically accelerate the particle's degradation during high-voltage cycling.

In addition, it is interesting to point out that, for some particular NMC622 materials in this study, a hole can be observed at the center of secondary particle regardless of the cycling history. This feature could be introduced during synthesis process intentionally by the manufacturer to help buffer the strain and deformation in order to mitigate capacity fading during electrochemical cycling.[52] It has been reported that grains in the interior of the particle are easily isolated from the conducting network and deactivated, therefore, resulting in large capacity loss in the first few cycles.[47,48] The hole at the center of secondary particle may cause smaller packing density but might be able to suppress capacity loss in the first few cycles. Such a hollow design would also make the particles more robust against crack formation and propagation. To verify this hypostasis, a comparison of the tomographic results between a densely packed and a hollow NMC622 secondary particles is shown in **Figure 6** (the particle with and without hole at the center was selected from different sample batches using different synthesis procedures). It was observed that the closely packed particle is more severely damaged as it went through similar cycling history. Therefore, impedance spectroscopic measurement was performed, and the results are shown in Figure 6c. The results clearly show more rapid development of the impedance in the electrode made of particles without holes, suggesting the degradation of integrity, which is likely caused by severe particle cracking (see Figure S10, Supporting Information, for the virtual slices through the center of a cycled solid particle).

To understand the observed difference in the mechanical robustness between solid and hollow NMC622 particles, we employ finite element modeling to investigate the chemomechanical behavior of them. As shown in **Figure 7**, theoretical models are built by aggregating polygonal primary particles for both solid (without hole) and hollow NMC secondary particles. The mechanical deformation caused by Li extraction induces a field of stress within the secondary particles and facilitates the initiation and propagation of intergranular cracks. Figure 7a shows the profiles of equivalent stress distribution in the particles upon completion of charging. The solid NMC secondary particle clearly experiences a higher stress in both tension (red color) and compression (blue color) than the hollow particle. The difference is attributed to two reasons. One is that the empty space at the center of the hollow particle accommodates deformation and reduces the internal stress.[53] The other reason is that the shorter diffusion length within the hollow particle leads to a more homogeneous Li distribution which further reduces the mismatch strain. Figure 7b,c shows the evolution of Li concentration and hoop stress along the radial direction of the solid and hollow NMC particles as a function of the normalized charging time Dt/R^2, where R represents the radius of the NMC secondary particle. Upon delithiation, a gradient of Li concentration exists in both particles. The outer shell has a lower Li concentration than the core regime. As a result, the secondary particle is subject to a tensile stress near the surface and a compressive stress at the center. Because of the additional free surface and a more homogeneous Li distribution, the maximum tensile stress in the hollow particle is nearly 50% lower than that in the solid counterpart. This indicates that mechanical disintegration happens more likely in the solid NMC particle. The empty space at the center of hollow secondary particle helps in buffering the stress causing the disintegration of particles during cycling. Previously, the enhancement of secondary particle integrity was mostly achieved chemically such as surface coating and grain boundary protection.[54,55] The coating layer separates the cathode from electrolyte and, therefore, reduces solid–liquid interfacial reaction, suppresses intergranular cracking and surface structure degradation. Though the hollow structure could not completely prevent the cathode particle from contacting electrolyte, it helps to reduce crack formation by releasing the mechanical stresses induced by cycling and, therefore, decreasing the solid–liquid interfaces as well. Either mechanically or chemically, minimizing side reaction between cathode material and electrolyte would better preserve
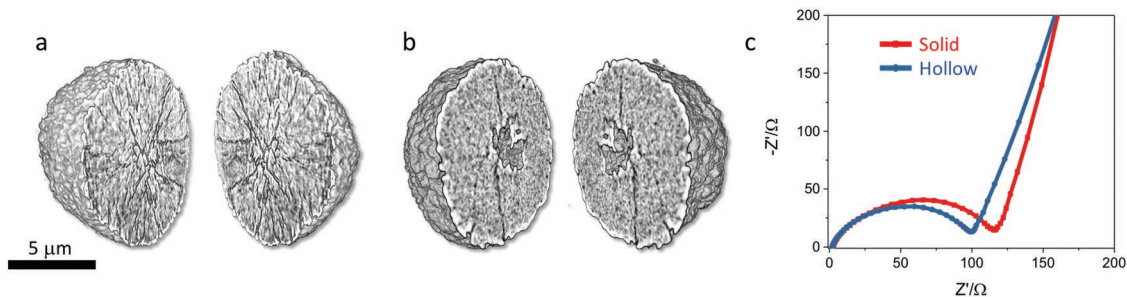

Figure 6. Comparison between the mechanical robustness of the solid and the hollow NMC secondary particle. a,b) Nano-resolution tomographic results of a solid NMC particle and a hollow one, both of which have gone through 30 electrochemical cycles with a rate of C/8. c) The electrochemical impedance spectroscopy result of the solid and hollow sample, respectively. The scale bar in (a) is 5 microns.
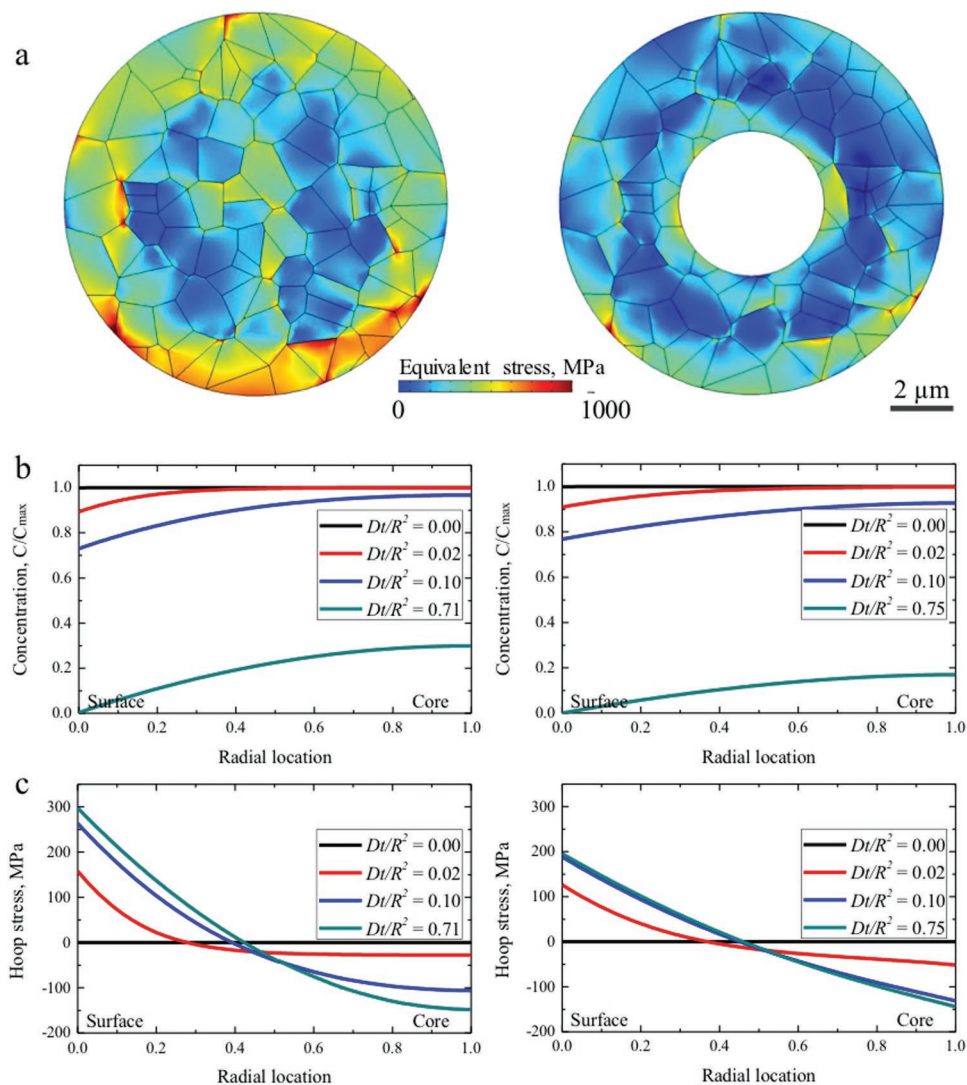
**ADVANCED
SCIENCE NEWS**
www.advancedsciencenews.com

**ADVANCED
FUNCTIONAL
MATERIALS**
www.afm-journal.de

Figure 7. Finite element modeling of the solid (left column) and hollow (right column) NMC secondary particles. a) The equivalent stress within the NMC particles upon completion of charging (Li extraction). The evolution of b) Li concentration and c) hoop stress within the NMC particles during charging.

the particle integrity during cycling. At the deep de-lithiation state, one may expect that cracks propagate from the surface toward the bulk because of the tensile stress generated near the surface (see the hoop stress profiles in Figure 7c). However, other factors, for instance, the presence of initial defects, the heterogeneous contact of NMC particles with the conductive network, liquid electrolyte infiltration, and surface reconstruction could all play certain roles in the crack formation and propagation. Therefore, whether the cracking is formed first at the surface or in the bulk is a complicated problem. We hope to discuss this important issue in detail in another future work. These results provide valuable information about the engineering design of the material synthesis. The morphology of the synthesized material (with or without hole at the center of the secondary particles) is also very important and a balance between the high packing density and the structural integrity against prolonged cycling, especially at high-voltage charging is needed.

3. Conclusion

In this work, the NMC622 cathode particles that were cycled extensively over different voltage windows were studied. While the bulk averaged X-ray diffraction technique revealed that the overall NMC lattice structure changes are highly reversible, the elementally specific X-ray spectroscopy suggested that the local structure around Ni cation is more severely disordered upon cycling to high charge cut-off voltage. For better understanding of such effect, we conducted a nano-resolution X-ray spectro-microscopic study of the particles that have gone through different cycling histories. We developed a hybrid supervised and unsupervised machine-learning approach to identify and visualize the chemical outliers in the NMC secondary particles. We observed that more-reduced and more-oxidized domains coexist in the particle. These chemical outliers are attributed to different unwanted side reactions. The more-reduced domains are likely to be rock salt structure

and mostly occur at the surface, building up the impedance. The more-oxidized domains occur in the bulk, leading to local deactivation of isolated domains. We further investigated the 3D morphological defects within the secondary particles and proposed that the degree of particle cracking can be tuned by carefully engineering the as-made particle morphology. The work presented in this manuscript offers valuable insights into the particle-level degradation mechanism when cycled to high charge cut-off voltage, which is very important from both fundamental and practical perspectives. The machine-learning approach developed is also applicable to a wide range of research fields well beyond battery science.

Supporting Information

Supporting Information is available from the Wiley Online Library or from the author.

Conflict of Interest

The authors declare no conflict of interest.

[1] D. Larcher, J. M. Tarascon, *Nat. Chem.* **2015**, *7*, 19.
[2] A. Manthiram, B. Song, W. Li, *Energy Storage Mater.* **2017**, *6*, 125.
[3] S.-T. Myung, F. Maglia, K.-J. Park, C. S. Yoon, P. Lamp, S.-J. Kim, Y.-K. Sun, *ACS Energy Lett.* **2017**, *2*, 196.
[4] T. Ohzuku, Y. Makimura, *Chem. Lett.* **2001**, *30*, 642.
[5] L. Wang, J. Li, X. He, W. Pu, C. Wan, C. Jiang, *J. Solid State Electrochem.* **2009**, *13*, 1157.
[6] W. Liu, P. Oh, X. Liu, M.-J. Lee, W. Cho, S. Chae, Y. Kim, J. Cho, *Angew. Chem., Int. Ed.* **2015**, *54*, 4440.
[7] J. Choi, A. Manthiram, *J. Electrochem. Soc.* **2005**, *152*, A1714.
[8] L. Mu, R. Lin, R. Xu, L. Han, S. Xia, D. Sokaras, J. D. Steiner, T.-C. Weng, D. Nordlund, M. M. Doeff, Y. Liu, K. Zhao, H. L. Xin, F. Lin, *Nano Lett.* **2018**, *18*, 3241.
[9] H. Lu, H. Zhou, A. M. Svensson, A. Fossdal, E. Sheridan, S. Lu, F. Vullum-Bruer, *Solid State Ionics* **2013**, *249–250*, 105.
[10] M.-H. Kim, H.-S. Shin, D. Shin, Y.-K. Sun, *J. Power Sources* **2006**, *159*, 1328.
[11] J. Li, L. E. Downie, L. Ma, W. Qiu, J. R. Dahn, *J. Electrochem. Soc.* **2015**, *162*, A1401.
[12] S.-K. Jung, H. Gwon, J. Hong, K.-Y. Park, D.-H. Seo, H. Kim, J. Hyun, W. Yang, K. Kang, *Adv. Energy Mater.* **2014**, *4*, 1300787.
[13] H.-H. Ryu, K.-J. Park, C. S. Yoon, Y.-K. Sun, *Chem. Mater.* **2018**, *30*, 1155.
[14] M. Guilmard, L. Croguennec, C. Delmas, *Chem. Mater.* **2003**, *15*, 4484.
[15] I. Saadoune, D. Claude, *J. Mater. Chem.* **1996**, *6*, 193.
[16] E. Zhecheva, R. Stoyanova, *Solid State Ionics* **1993**, *66*, 143.
[17] Y. Cho, J. Cho, *J. Electrochem. Soc.* **2010**, *157*, A625.
[18] D. R. Gallus, R. Schmitz, R. Wagner, B. Hoffmann, S. Nowak, I. Cekic-Laskovic, R. W. Schmitz, M. Winter, *Electrochim. Acta* **2014**, *134*, 393.
[19] K. S. Kang, S. Choi, J. Song, S.-G. Woo, Y. N. Jo, J. Choi, T. Yim, J.-S. Yu, Y.-J. Kim, *J. Power Sources* **2014**, *253*, 48.
[20] K. S. Lee, S. T. Myung, K. Amine, H. Yashiro, Y. K. Sun, *J. Electrochem. Soc.* **2007**, *154*, A971.
[21] H. Zheng, Q. Sun, G. Liu, X. Song, V. S. Battaglia, *J. Power Sources* **2012**, *207*, 134.
[22] Y. Xu, E. Hu, K. Zhang, X. Wang, V. Borzenets, Z. Sun, P. Pianetta, X. Yu, Y. Liu, X.-Q. Yang, H. Li, *ACS Energy Lett.* **2017**, *2*, 1240.
[23] K. Zhang, F. Ren, X. Wang, E. Hu, Y. Xu, X.-Q. Yang, H. Li, L. Chen, P. Pianetta, A. Mehta, X. Yu, Y. Liu, *Nano Lett.* **2017**, *17*, 7782.
[24] W. E. Gent, Y. Li, S. Ahn, J. Lim, Y. Liu, A. M. Wise, C. B. Gopal, D. N. Mueller, R. Davis, J. N. Weker, J.-H. Park, S.-K. Doo, W. C. Chueh, *Adv. Mater.* **2016**, *28*, 6631.
[25] H. Zhang, F. Omenya, P. Yan, L. Luo, M. S. Whittingham, C. Wang, G. Zhou, *ACS Energy Lett.* **2017**, *2*, 2607.
[26] F. Lin, I. M. Markus, D. Nordlund, T.-C. Weng, M. D. Asta, H. L. Xin, M. M. Doeff, *Nat. Commun.* **2014**, *5*, 3529.
[27] E. Hu, X. Wang, X. Yu, X.-Q. Yang, *Acc. Chem. Res.* **2018**, *51*, 290.
[28] F. Meirer, J. Cabana, Y. Liu, A. Mehta, J. C. Andrews, P. Pianetta, *J. Synchrotron Radiat.* **2011**, *18*, 773.
[29] H.-J. Noh, S. Youn, C. S. Yoon, Y.-K. Sun, *J. Power Sources* **2013**, *233*, 121.
[30] W. Zhao, J. Zheng, L. Zou, H. Jia, B. Liu, H. Wang, M. H. Engelhard, C. Wang, W. Xu, Y. Yang, J.-G. Zhang, *Adv. Energy Mater.* **2018**, *8*, 1800297.
[31] J. Kasnatscheew, M. Evertz, B. Streipert, R. Wagner, S. Nowak, I. Cekic Laskovic, M. Winter, *J. Power Sources* **2017**, *359*, 458.
[32] D. J. Kautz, L. Tao, L. Mu, D. Nordlund, X. Feng, Z. Zheng, F. Lin, *J. Mater. Chem. A* **2018**, *6*, 16003.
[33] Y. Ruan, X. Song, Y. Fu, C. Song, V. Battaglia, *J. Power Sources* **2018**, *400*, 539.
[34] K. H. Jeong, H.-W. Ha, N. J. Yun, M. Z. Hong, K. Kim, *Electrochim. Acta* **2005**, *50*, 5349.
[35] S.-T. Myung, S. Komaba, N. Hirosaki, H. Kosoya, N. Kumagai, *J. Power Sources* **2005**, *146*, 645.
[36] T. Ohzuku, A. Ueda, M. Nagayama, *J. Electrochem. Soc.* **1993**, *140*, 1862.
[37] G. K. Williamson, W. H. Hall, *Acta Metall.* **1953**, *1*, 22.
[38] R. Xu, L. Vasconcelos, J. Shi, J. Li, K. Zhao, *Exp. Mech.* **2018**, *58*, 549.

**ADVANCED
SCIENCE NEWS**

www.advancedsciencenews.com

**ADVANCED
FUNCTIONAL
MATERIALS**

www.afm-journal.de

[39] C. Tian, D. Nordlund, H. L. Xin, Y. Xu, Y. Liu, D. Sokaras, F. Lin, M. M. Doeff, *J. Electrochem. Soc.* **2018**, *165*, A696.

[40] X. L. Wang, K. An, L. Cai, Z. Feng, S. E. Nagler, C. Daniel, K. J. Rhodes, A. D. Stoica, H. D. Skorpenske, C. Liang, W. Zhang, J. Kim, Y. Qi, S. J. Harris, *Sci. Rep.* **2012**, *2*, 747.

[41] Q. Wang, C. H. Shen, S. Y. Shen, Y. F. Xu, C. G. Shi, L. Huang, J. T. Li, S. G. Sun, *ACS Appl. Mater. Interfaces* **2017**, *9*, 24731.

[42] E. Hu, X. Yu, R. Lin, X. Bi, J. Lu, S. Bak, K.-W. Nam, H. L. Xin, C. Jaye, D. A. Fischer, K. Amine, X.-Q. Yang, *Nat. Energy* **2018**, *3*, 690.

[43] A. Mukhopadhyay, B. W. Sheldon, *Prog. Mater. Sci.* **2014**, *63*, 58.

[44] C. Wei, S. Xia, H. Huang, Y. Mao, P. Pianetta, Y. Liu, *Acc. Chem. Res.* **2018**, *51*, 2484.

[45] X. Duan, F. Yang, E. Antono, W. Yang, P. Pianetta, S. Ermon, A. Mehta, Y. Liu, *Sci. Rep.* **2016**, *6*, 34406.

[46] J. Nelson Weker, A. M. Wise, K. Lim, B. Shyam, M. F. Toney, *Electrochim. Acta* **2017**, *247*, 977.

[47] D. J. Miller, C. Proff, J. G. Wen, D. P. Abraham, J. Bareño, *Adv. Energy Mater.* **2013**, *3*, 1098.

[48] H.-H. Sun, A. Manthiram, *Chem. Mater.* **2017**, *29*, 8486.

[49] C. S. Yoon, D.-W. Jun, S.-T. Myung, Y.-K. Sun, *ACS Energy Lett.* **2017**, *2*, 1150.

[50] P. Yan, J. Zheng, M. Gu, J. Xiao, J.-G. Zhang, C.-M. Wang, *Nat. Commun.* **2017**, *8*, 14101.

[51] S. Watanabe, M. Kinoshita, T. Hosokawa, K. Morigaki, K. Nakura, *J. Power Sources* **2014**, *258*, 210.

[52] J. Kim, H. Cho, H. Y. Jeong, H. Ma, J. Lee, J. Hwang, M. Park, J. Cho, *Adv. Energy Mater.* **2017**, *7*, 1602559.

[53] K. Zhao, M. Pharr, L. Hartle, J. J. Vlassak, Z. Suo, *J. Power Sources* **2012**, *218*, 6.

[54] B. Xiao, H. Liu, J. Liu, Q. Sun, B. Wang, K. Kaliyappan, Y. Zhao, M. N. Banis, Y. Liu, R. Li, T. K. Sham, G. A. Botton, M. Cai, X. Sun, *Adv. Mater.* **2017**, *29*, 1703764.

[55] P. Yan, J. Zheng, J. Liu, B. Wang, X. Cheng, Y. Zhang, X. Sun, C. Wang, J.-G. Zhang, *Nat. Energy* **2018**, *3*, 600.